Co-deletion of Lrp5 and Lrp6 in the skeleton severely diminishes bone gain from sclerostin antibody administration

Authors: Kyung-Eun Lim[1], Whitney A. Bullock[1], Daniel J. Horan[1], Bart O. Williams[2], Matthew L. Warman[3], and Alexander G. Robling[1,4,5,6]*

Affiliations:

[1]Department of Anatomy, Cell Biology & Physiology, Indiana University School of Medicine, Indianapolis, IN, USA

[2]Program for Skeletal Disease and Tumor Microenvironment, Center for Cancer and Cell Biology, Van Andel Research Institute, Grand Rapids, MI, USA

[3]Department of Orthopaedic Surgery, Boston Children's Hospital, Boston, MA, USA

[4]Department of Biomedical Engineering, Indiana University–Purdue University at Indianapolis, Indianapolis, IN, USA

[5]Richard L. Roudebush VA Medical Center, Indianapolis, IN, USA

[6]Indiana Center for Musculoskeletal Health, Indianapolis, IN, USA

Running Head: sclerostin antibody treatment in Lrp5/6-deficient mice

Keywords: Wnt, sclerostin, Sost, Lrp5, Lrp6, osteocytes, osteoporosis

Disclosure Statement: The authors have nothing to disclose.

***Corresponding Author**:

Alexander G. Robling, Ph.D.
Department of Anatomy, Cell Biology & Physiology
Indiana University School of Medicine
635 Barnhill Dr., MS 5035
Indianapolis, IN 46202
Tel: (317) 274-7489
Fax: (317) 278-2040
Email: arobling@iupui.edu

Grant support:

This work was supported by NIH grant AR053237 (to AGR and MLW) and VA grant BX001478 (to AGR).

Abstract

The cysteine knot protein sclerostin is an osteocyte-derived secreted inhibitor of the Wnt co-receptors LRP5 and LRP6. LRP5 plays a dominant role in bone homeostasis, but we previously reported that Sost/sclerostin suppression significantly increased osteogenesis regardless of Lrp5 presence or absence. Those observations suggested that the bone forming effects of sclerostin inhibition can occur through Lrp6 (when Lrp5 is suppressed), or through other yet undiscovered mechanisms independent of Lrp5/6. To distinguish between these two possibilities, we generated mice with compound deletion of Lrp5 and Lrp6 selectively in bone, and treated them with sclerostin monoclonal antibody (Scl-mAb). All mice were homozygous flox for both Lrp5 and Lrp6 ($Lrp5^{f/f}$; $Lrp6^{f/f}$), and varied only in whether or not they carried the Dmp1-Cre transgene. Positive (Cre+) and negative (Cre-) mice were injected with Scl-mAb or vehicle from 4.5–14 wks of age. Vehicle-treated Cre+ mice exhibited significantly reduced skeletal properties compared to vehicle-treated Cre- mice, as assessed by DXA, μCT, pQCT, and histology, indicating that Lrp5/6 deletions were effective and efficient. Scl-mAb treatment improved nearly every bone-related parameter among Cre- mice, but the same treatment in Cre+ mice resulted in little to no improvement in skeletal properties. For the few endpoints where Cre+ mice responded to Scl-mAb, it is likely that antibody-induced promotion of Wnt signaling occurred in cell types earlier in the mesenchymal/osteoblast differentiation pathway than the Dmp1-expressing stage. This latter conclusion was supported by changes in some histomorphometric parameters. In conclusion, unlike with the deletion of Lrp5 alone, the bone-selective late-stage co-deletion of Lrp5 and Lrp6 significantly impairs or completely nullifies the osteogenic action of Scl-mAb, and highlights a major role for both Lrp5 and Lrp6 in the mechanism of action for the bone-building effects of sclerostin antibody.

Low bone mass is a growing problem among the expanding senescent population worldwide.[1] Nearly half of all women in the US will experience an osteoporosis-related fracture at some point in their lifetime.[2] Preventing bone loss, particularly among postmenopausal women, has been a major focus of skeletal drug discovery efforts over the past 25 years. While the most progress has been made in the development and delivery of anti-resorptive agents, that focus has shifted in recent years toward the development of bone-building therapeutics. Within the past three years, the FDA has approved two new bone forming agents—the PTHrP analog abaloparatide and the sclerostin antibody romosozumab-aqqg (romo). Both of these agents result in net bone gain and reduce fracture risk significantly.[3,4]

One of the most promising pathways to exploit for building new bone is the Wnt signaling pathway, which is the pathway exploited in the identification and development of romo. Romo blocks the action of its target, sclerostin, from interacting with and inhibiting the Wnt co-receptors LRP5 and LRP6. Insight into sclerostin's function in bone came from two main clinical populations: sclerosteosis patients who harbor loss-of-function mutations in the SOST gene,[5,6] and hyperostosis corticalis patients who harbor gain-of function mutations in the sclerostin target LRP5.[7,8] Both of these patient populations have very high bone mass, and in both cases the mechanism of action is presumed to be at least partially explained by compromised sclerostin:LRP5 interaction.[9,10] In the case of sclerosteosis, no functional sclerostin is produced and consequently the sclerostin:LRP5 interaction is compromised. In the case of hyperosteosis corticalis, the LRP5 receptor has an amino acid substitution that dramatically reduces sclerostin affinity, and consequently the sclerostin:LRP5 interaction is compromised. Both scenarios lead to a high bone mass (HBM) phenotype, and mouse models engineered to harbor respective species-orthologous Lrp5[11] and Sost[12] mutations roughly phenocopy one another.[13]

It is curious to note that LRP5-HBM patients have high bone mass despite having normal alleles for LRP6 (which are susceptible to sclerostin-mediated inhibition) and a concomitant increase in circulating sclerostin levels, which would presumably further impair the susceptible LRP6 receptor.[14] As impaired Lrp6 function has severe consequences for bone mass,[15] those observations taken together could suggest that LRP6 might not be involved in the anabolic program in bone, a notion for which there is at least some experimental evidence.[16] The idea that LRP5 mediates the anabolic action of sclerostin deficiency was tested in a previous communication, where $Lrp5^{-/-}$ mice were either treated with sclerostin antibody, or, in separate experiments, cross-bred onto a $Sost^{-/-}$ background.[17] We expected to find no bone-building effects of Sost/sclerostin deficiency when tested in the $Lrp5^{-/-}$ mice, since it seemed likely (for the reasons outlined above) that the anabolic effects of sclerostin inhibition were mediated by Lrp5. To the contrary, $Lrp5^{-/-}$ mice experienced significant osteoanabolic action in the context of Sost deletion and sclerostin neutralization. That result begged the question of whether bone building effects of sclerostin inhibition were mediated by Lrp6 (perhaps in a compensatory manner when Lrp5 is disabled), or alternatively, whether sclerostin has other anti-osteoanabolic targets that might be driving the effect. In support of the former, LRP6 can substitute functionally for LRP5 in *in vitro* Wnt signaling assays,[10,18] and can bind and be inhibited by sclerostin.[19,20] In support of the latter, several non-Lrp5/6 binding partners have been identified for sclerostin in *in vitro* experiments including BMPs, noggin, Ccn1, Egfr-3, Alp, carbonic anhydrase, gremlin-1, Ahsg, Mdk, Anxa-1 & -2, Col-I, Ck2, and sFrp4.[21-24]

To address this conundrum, we deleted both Lrp5 and Lrp6 from late-stage skeletal cells of mice, using floxed loss-of-function alleles for both Lrp5 and Lrp6 and the Dmp1-Cre driver. The mice were treated with sclerostin antibody to induce anabolic action, and the skeletal response was evaluated. In short, mice with compound Lrp5 and Lrp6 loss in the osteocyte/osteoblast population had severely compromised bone gain in response to Scl-mAb, similar to vehicle-treated mutant mice. The results suggest that the vast majority of the bone-building effects of sclerostin neutralization occur mechanistically through the Wnt co-receptors Lrp5/6.

Materials and Methods

Mice: Development of the conditional Lrp5 and Lrp6 mouse models has been reported elsewhere.[25] Briefly, loxP sites were introduced into the introns flanking exon 2 of Lrp5 and Lrp6 using homologous recombination. Development of the ^{10kb}Dmp1-Cre transgenic mouse model has been reported elsewhere.[26] Briefly, these mice harbor a transgene expressing Cre recombinase driven by a 9.6kb fragment of the mouse Dentin Matrix Protein-1 promoter. All mouse colonies were maintained on a C57BL/6J background. For all experiments, mice were compound homozygous flox ($Lrp5^{f/f}$;$Lrp6^{f/f}$), and only differed by whether or not they carried the Dmp1-Cre transgene. Mice were sacrificed at 14.5 wks of age. All mouse procedures were performed in accordance with the IACUC guidelines and approvals.

Antibody treatment: Details of the development of sclerostin-neutralizing antibody (provided by Amgen, Inc.) has been reported elsewhere.[27] Briefly, the sclerostin antibody (Scl-Ab) is a ratized version of a mouse monoclonal antibody that neutralizes mouse sclerostin. Scl-Ab was injected into mice subQ at 25 mg/kg, 200 µL per injection, twice per week for 10 weeks, beginning at 4.5 wks of age. Vehicle treatment was the saline buffer in which the antibodies were made, and was injected with identical frequency, volume, and duration as described for antibody injections.

Dual-energy x-ray absorptiometry (DXA): Collection of serial DXA measurements on live mice are described and validated elsewhere.[17] Briefly, mice were anesthetized via inhalation of 2.5% isoflurane (IsoFlo; Abbott Laboratories, North Chicago, IL) mixed with O_2 (1.5 liter/min) for a total ~8 min, including both induction and scanning. The mice were placed in prone position on a specimen tray within the scanner. Whole body scans were analyzed regionally using the Lunar region of interest (ROI) tools. The ROI for the spine included from the third (LV_3) through fifth (LV_5) lumbar vertebrae. The ROI for the hindlimb included all skeletal tissue distal the acetabulum. The ROI for the whole body included all skeletal tissues caudal to the first cervical/occipital boundary. Serial scans were performed at 4, 6.5, 9.5, 12.5, and 14 weeks of age. Bone mineral density (BMD) and content (BMC) was measured for each ROI scan.

Micro–computed tomography (µCT): Formalin fixed femora and 5th lumbar vertebrae were scanned, reconstructed, and analyzed as previously described.[17] Briefly, 10 µm resolution, 50-kV peak tube potential and 151-ms integration time were used to collect scans on a Scanco uCT-35 tomographer. The distal 60% of each femur and the entire body of each vertebra were scanned. Standard parameters related to cancellous and cortical bone architecture were measured.[28]

Peripheral quantitative micro-computed tomography (pQCT): Collection of serial tibial pQCT measurements in live mice is described elsewhere.[29] Briefly, a single slice through the proximal tibia, located 4 mm distal to the intercondylar eminence, was collected on isoflurane-anesthetized mice using a Stratec x-ray µScope (Stratec Inc.) at 70-µm resolution. Slices were analyzed for bone mineral density using Stratec software in peel mode 2.

Fluorochrome administration, bone quantitative histomorphometry, and histology: All mice were given 200µL injections of calcein (12 mg/kg, i.p.) at 4 wks, oxytetracycline (60 mg/kg subQ) at 6.5 wks, alizarin complexone (20 mg/kg, i.p.) at 9.5 wks, and demeclocycline (10 mg/kg subQ) at 12.5 wks to periodically label mineralizing bone throughout the experimental period. After sacrifice at 14.5 wks of age, the femurs were processed, for plastic-embedded histomorphometry and cut at midshaft for histological evaluation as previously described.[30] Briefly, periosteal and endocortical bone formation rates (BFR/BS; $\mu m^3/\mu m^2$/day), mineral apposition rates (MAR; µm/day) and mineralizing

surface (MS/BS; %) were calculated from sequential pairs of labels laid down throughout the experimental period, using standard protocols.[31] Tartrate resistant acid phosphatase (Trap) staining for osteoclasts was conducted on decalcified proximal tibia thin sections as previously described.[32]

Serum ELISAs: Serum concentration of the resorption marker collagen C-terminal telopeptide (CTX) and the bone formation inhibitor sclerostin was measured by commercially available ELISAs (RatLaps; IDS Inc. for CTX and Quantikine; R&D Systems, Inc., for sclerostin) as previously described.[17,30,33] Briefly, blood samples were collected from O/N fasted 4-wk-old mice (just prior to initiation of the antibody course) at the retromandibular vein, and again 2 weeks after beginning antibody treatment. Blood samples were permitted to clot at room temperature for 30 minutes, spun at 5,000 g to separate the serum, and frozen at –80°C. Thawed serum samples were assayed for CTX and sclerostin in duplicate or triplicate according to the manufacturer's instructions.

Statistics: Statistical analyses were computed with JMP (version 12.0, SAS Institute Inc.). The tomography and serum biomarker endpoints were analyzed with 2-way ANOVA within sex, using Cre status and injection treatment as main effects. When at least one main effect was significant, interactions terms were calculated and tested for significance. Time series data were analyzed with repeated-measures ANOVA. Statistical significance was taken at $p < 0.05$. Two-tailed distributions were used for all analyses. Data are presented as mean ± SEM. A minimum of 8 animals was included in each group (*n*=8-11/group).

Results

Mice with compound Lrp5/Lrp6 loss-of-function alleles in Dmp1-expressing cells are severely osteopenic and have global and regional deficits in Scl-mAb-stimulated bone mineral accrual.

Our previous work, showing potent anabolic action of sclerostin antibody in $Lrp5^{-/-}$ mice,[17] suggested that sclerostin inhibition might increase bone mass through Lrp6 activation, or perhaps through alternative pathways that do not require Lrp5 or Lrp6 activation. To test this idea, we administered twice-weekly Scl-mAb injections to 4-wk-old mice deficient in both Lrp5 and Lrp6 in bone, and measured the skeletal response using serial DXA scans collected over the subsequent 10-wk antibody treatment period. The Cre strategy was effective in recombining both Lrp5 and Lrp6 floxed alleles in bone tissue (Fig S1). Both Cre status and antibody exposure had significant effects on bone mineral content (BMC) at all regions of interest (ROIs; whole body, spine, hindlimb). The interaction between Cre and antibody was also statistically significant for every ROI with the exception of hindlimb BMC among male mice, indicating that Lrp5/6 deletion from bone has a significant effect on response to antibody treatment. Probing individual group comparisons, deletion of Lrp5/6 induced a significant decrease (as expected[34]) in BMC, which was consistently apparent at all ROIs by 6 wks of age or earlier (Fig. 1). Among WT (Cre-negative) mice, Scl-mAb induced a significant increase in bone mineral content (BMC) at every ROI examined, including whole body, lumbar spine, and hindlimb, compared to WT mice treated with vehicle. Among mutant (Cre-positive), mice, Scl-mAb induced significant BMC increases for some regions but not others. For example, BMC was increased by antibody treatment at the hindlimb (Fig. 1E & 1F) but not spine (Fig. 1C & 1D), and for whole body among males (Fig. 1A) but not females (Fig. 1B). The absolute gains in mineral content induced by antibody were 3.5 – 5.5 times greater among WT mice as compared to mutant mice, for whole body and spine ROIs, and 2.0 – 2.5 times greater among WT mice for the hindlimb. Body mass was affected by Cre status in both male and female mice but antibody affected body mass only among male mice (Fig. S2). In summary, Scl-mAb had potent effects on DXA-derived BMC in WT mice, but its efficacy was severely blunted or absent among mice with bone-selective deletion of Lrp5 and Lrp6.

Lrp5/6 conditional mutant mice have impaired cancellous and cortical bone properties, with blunted or undetectable response to Scl-mAb.

To probe compartment-specific effects of the Lrp5/6 compound mutations in bone, and the response to Scl-mAb in Lrp5/6 compromised mice, the femur and spine from antibody-treated WT and mutant mice were scanned via μCT to collect distal femur and L_5 cancellous properties and midshaft femur cortical properties. Bone volume fraction (BV/TV) and trabecular thickness and number (Tb.Th and Tb.N) in the distal femur were significantly affected by Cre status and antibody exposure for most of the endpoints (Fig. 2A-2C, Fig S3). The interaction term (Cre × injection) was statistically significant for all endpoints among both sexes, indicating that Lrp5/6 deletion from bone has a significant effect on the cancellous bone response to antibody. Probing individual group comparisons, deletion of Lrp5/6 induced a significant decrease in Tb.N in both sexes and in BV/TV among males. Scl-mAb treatment significantly increased distal femur cancellous properties in WT but not mutant mice, with the exception of Tb.N among males.

Cortical properties in the femur were significantly affected by Cre status and antibody exposure (Fig. 2D-2F, Fig. S3). The interaction term (Cre × injection) was significant for all cortical properties except total area (Tt.Ar). Post-hoc testing revealed a Scl-mAb-stimulated increase in all cortical properties, regardless of Cre status, with the exception of Ct.Th among Cre-positive males.

In the 5th lumbar vertebra, BV/TV was significantly reduced in Cre-positive mice compared to Cre-negative mice (Fig. 3A, Fig. S4). Antibody was efficacious in increasing vertebral BT/TV only in Cre-negative mice. Vertebral Tb.N and Tb.Th measurements were highly variable in Cre-positive mice due to the near complete absence of trabecular bone (See Fig. 3B), which resulted in large pooled error terms (data not shown).

Longitudinal changes in bone properties were assess using in vivo pQCT at a cortical-rich site (the tibia mid-diaphysis) and a cancellous-rich site (the proximal tibial metaphysis). Three weeks after beginning antibody treatment, Cre-negative mice exhibited a significant increase in BMD at the tibial diaphysis but not at the tibial metaphysis (Fig. 4A-4B). Cre-positive mice exhibited no effect of antibody at the 3-wk time point at either site. Ten weeks after beginning antibody treatment, Cre-negative mice exhibited significant increases in BMD at both sites, whereas no changes could be detected in the Cre-positive mice. In summary, Scl-mAb had potent effects on μCT- and pQCT-derived properties in WT mice, but its efficacy was severely blunted or absent among mice with bone-selective deletion of Lrp5 and Lrp6.

Select cortical bone formation parameters that precede Cre activation are increased in Scl-mAb-treated Lrp5/6 conditional mutant mice.

The unexpected ability of Scl-mAb to increase Tt.Ar and B.Ar in the femoral midshaft among mice with conditional inactivation of Lrp5/6 (Fig. 2D-2E) prompted us to determine which, if any, bone formation parameters at that site were activated by Scl-mAb. We measured mineralizing surface, apposition rates, and formation rates using all 4 embedded labels, which permitted snapshots of bone formation during the 3 intervening periods (5 wks, 8 wks, and 11 wks). On the periosteal surface, Scl-mAb significantly increased mineralizing surface in both Cre-positive and Cre negative mice, but no changes in mineral apposition rates were detected (Fig. 5B-5D). The changes in MS/BS drove a significant increase in periosteal bone formation rates (BFR/BS) among Cre-positive mice, whereas the increase in BFR/BS among Cre-negative mice failed to reach significance ($p=0.07$). The same measurements at the endocortical surface yielded significant increases in MS/BS and BFR/BS for Cre-negative but not Cre-positive mice (Fig. 5E-5G). Serum measurements of the resorption biomarker collagen c-terminal telopeptide (CTX) were not different among mice at the start of the experiment, nor after 2.5 wks of antibody or vehicle treatment (Fig. 6). Quantitative histological evaluation of osteoclast surface could not be accomplished because of the lack of trabecular in two of the groups (Fig. S5). However, serum sclerostin levels were significantly reduced in Cre-positive mice prior to treatment, and antibody treatment in both Cre+ and Cre- mice resulted in a similar, 15× increase in sclerostin levels after 2.5 wks of treatment (Fig. S6). In summary, Scl-mAb increased mineralizing surface on the periosteum in both WT and mutant mice, but the endocortical surface was stimulated by antibody only in WT mice.

Discussion

In a previous communication[17] we reported that Lrp5$^{-/-}$ mice respond robustly to sclerostin antibody, similar to the response found in their WT littermates. Further, Lrp5$^{-/-}$ mice bred onto a Sost$^{-/-}$ background had significantly improved cancellous and cortical bone properties compared to Lrp5$^{-/-}$ littermates. Those two results suggest that (1) Lrp5 might not be important for transducing the anabolic response to Sost/sclerostin inhibition, and that the bone building effects of sclerostin inhibition are mediated mainly by Lrp6; (2) that Lrp5 is normally important for the response to Sost/sclerostin inhibition, but that Lrp6 can substitute for Lrp5 when Lrp5 is disabled; or (3) that some of the bone building effects of sclerostin inhibition are transduced through collateral transduction pathways other than Wnt/Lrp5/6. In this communication, our experiments were designed to test the efficacy of sclerostin inhibition when both Lrp5 and Lrp6 were deleted in bone (option 2 above). We found that for most endpoints, mice deficient in Lrp5/6 did not respond to Scl-mAb, suggesting that sclerostin's action on Lrp5/6 explains nearly all of the bone-building effects of sclerostin inhibition. We therefore reject the alternate hypothesis sclerostin inhibition promotes bone formation through signaling pathways other than Wnt (such as BMP). Our observations are consistent with a previous investigation in which Lrp5$^{-/-}$;Sost$^{-/-}$ mice were given an Lrp6 antibody and bone gain was further reduced.[35] Whereas their work inhibited the 1st β-propeller and spared the Dkk1- and Wnt3a-class-interacting 3rd β-propeller, our study took out all domains of the protein. Further, our results suggest that our previous report of full anabolic action of Scl-mAb in Lrp5$^{-/-}$ mice was likely due to Lrp6 substitution for Lrp5, in the genetic absence of functional Lrp5. We did not test Scl-mAb in mice with deletion of Lrp6 alone (i.e., Lrp5$^{+/+}$; Lrp6$^{f/f}$) because previous human and mouse studies focusing on the HBM-causing missense mutations in LRP5/Lrp5 already highlight the importance of Lrp5 in mediating sclerostin inhibition of bone formation.

We chose the Dmp1-Cre driver for these experiments because our previous work revealed that conditional gain-and loss-of-function Lrp5 alleles that are recombined with Dmp1-Cre result in phenocopy of global Lrp5-HBM and Lrp5$^{-/-}$ mice, respectively.[11] Further, comparison of vehicle treated Cre-negative mice (WT) with vehicle treated Cre-positive mice (mutant) yielded severe osteopenia in nearly every measurement collected, which indicates that the Dmp1-Cre is an appropriate driver to reveal the effects of Lrp5/6 signaling in bone. The drawback to using such a driver so late in the osteoblast differentiation pathway is that some of the effects of Scl-mAb on proliferation and differentiation might escape modulation of Dmp1-Cre mediated recombination of Lrp5/6. This is likely to have occurred in our experiment. For example, inspection of the histomorphometric data (Fig. 5) shows that the mineralizing surface but not apposition rate was positively affected by antibody in the mutant mice. Mineralizing surface reflects the recruitment and differentiation of osteoblast progenitors to the bone surface or re-activation of resident quiescent bone lining cells,[36] whereas MAR reflects the activity of individual, fully differentiated and mature osteoblasts. Because Dmp1 is not active at the differentiation stage that increases cell populations on the bone surfaces, it is likely that the increase in MS/BS preceded the Dmp1-Cre mediated recombination of the floxed alleles. Therefore, one interpretation of both the DXA data and femoral cortical data showing some effects of antibody in mutant mice might be attributable to Scl-mAb action on cell populations in which Lrp5/6 was not yet recombined. That would explain the DXA effects, particularly those ROIs

that are dominated by cortical bone (e.g. hindlimb but not spine). Repeating the experiment using the Prx1-Cre driver, which recombines in the limbs much earlier than Dmp1-Cre, might more fully address the residual effects of Scl-mAb in Lrp5/6 mutant mice.

Other limitations of the study include (1) off-target effects of the Dmp1-Cre driver, which has been documented in hypertrophic chondrocytes and might explain the absence of primary and secondary cancellous bone, and (2) that the recombination strategy did not conform to potential differences between cell populations/stages in which Lrp5 and Lrp6 are most active. Lrp6 has been reported to function earlier in the osteoblast differentiation pathway, whereas Lrp5 is active later.[34] Moreover, Lrp6 might have more of an influence on cancellous bone, and Lrp5 more on cortical bone. We were unable to account for these spatiotemporal differences in the two receptors using recombination strategy employed, and opted to delete both Lrp5 and Lrp6 in the late-stage osteoblast and osteocyte.

Regardless of the mechanism of action, a sclerostin antibody has been approved by the FDA and other regulatory agencies. Understanding the receptors that are targeted, off-target effects, and other molecular interactions will usher in refined approaches to improving bone gain in temporal and spatially controlled ways.

Figure Captions

Figure 1: Serial *in vivo* DXA scans of Cre-negative (triangles) and ^{10kb}Dmp1-Cre positive (circles) Lrp5$^{f/f}$;Lrp6$^{f/f}$ compound mice. Scans were collected every 2.5-3 wks and analyzed for (**A** & **B**) whole body bone mineral content (BMC), (**C** & **D**) lumbar spine BMC, and (**E** & **F**) right hindlimb BMC. Left panels display data from male mice; right panels display data from female mice. Antibody (dashed lines) and vehicle (solid lines) treatment began at 4.5 wks of age and lasted the duration of the experiment (to 14 wks of age). The longitudinal data were tested for significance within sex, between Cre status, using two-way rmANOVA. P-values for individual main effects and for the interaction term are presented in each panel. Tukey's HSD post hoc tests were used to compare among groups. *p<0.05 for comparison to respective vehicle-treated group (within Cre genotype). †p<0.05 for comparison between vehicle-treated groups (testing for genotype difference among vehicle-treated groups). *n*=7-9/time point/group for males; and *n*=8-13/time point/group for females.

Figure 2: µCT-derived measurement of the distal femur metaphyseal cancellous bone and mid-femur cortical bone from male Cre-negative and ^{10kb}Dmp1-Cre positive Lrp5$^{f/f}$;Lrp6$^{f/f}$ compound mice at 14.5 wks of age, treated with (mAb) or without (veh) sclerostin antibody for 10 wks prior to sacrifice. Quantitative differences in distal femur (**A**) trabecular bone volume fraction (BV/TV); (**B**), trabecular thickness (Tb.Th), and (**C**) trabecular number (Tb.N). Quantitative differences in midshaft femur cortical bone (**D**) total area (Tt.Ar), (**E**) bone area (B.Ar), and (**F**) cortical thickness. (**G**) Representative 3D reconstructions of (top row) the midshaft femur, (middle row) the distal metaphysis (proximal view), and (bottom row) the caudal half of the distal femur (the ventral half was digitally removed). Female data and reconstructions are presented in Fig. S3. Data were tested for significance using two-way ANOVA, with Cre status and injection type as main effects. P-values for individual main effects and for the interaction term are presented in each panel. Tukey's HSD post hoc tests were used to compare among groups. *p<0.05 for comparison to respective vehicle-treated group (within Cre genotype). †p<0.05 for comparison between vehicle-treated groups (testing for genotype difference among vehicle-treated groups). *n*=7-8/group.

Figure 3: µCT-derived measurement of the 5th lumbar (L5) vertebral body cancellous bone from male Cre-negative and ^{10kb}Dmp1-Cre positive Lrp5$^{f/f}$;Lrp6$^{f/f}$ compound mice at 14.5 wks of age, treated with (mAb) or without (veh) sclerostin antibody for 10 wks prior to sacrifice. (**A**) Quantitative differences in 5th lumbar trabecular bone volume fraction (BV/TV). Too little trabecular bone was present to take meaningful trabecular thickness and number measurements via µCT. (**B**) Representative 3D cutaway reconstructions of the 5th lumbar vertebra in rostro-caudal view (top row) and dorsoventral view (bottom row). Female data and reconstructions are presented in Fig. S4. Data were tested for significance using two-way ANOVA, with Cre status and injection type as main effects. P-values for individual main effects and for the interaction term are presented in each panel. Tukey's HSD post hoc tests were used to compare among groups. *p<0.05 for comparison to respective vehicle-treated group (within Cre genotype). †p<0.05 for comparison between vehicle-treated groups (testing for genotype difference among vehicle-treated groups). *n*=7-8/group.

Figure 4: pQCT-derived serial measurement of the right tibia in male Cre-negative and ^{10kb}Dmp1-Cre positive Lrp5$^{f/f}$;Lrp6$^{f/f}$ compound mice at 7 (left side of each data panel) and 14.5 (right side of each data panel) wks of age, treated with (mAb) or without (veh) sclerostin antibody beginning at 4.5 wks of age. Quantitative differences in (**A**) tibial midshaft bone mineral density (BMD), and (**B**) proximal tibial metaphyseal BMD. (**C**) Representative tomographic density heat map slices through the proximal (top row) and midshaft (bottom row) sites. Data were tested for significance using two-way ANOVA within each time point, with Cre status and injection type as main effects. P-values for individual main effects and for the interaction term are presented in each panel. Tukey's HSD post hoc tests were used to compare among groups. *p<0.05 for comparison to respective vehicle-treated group (within Cre genotype). †p<0.05 for comparison between vehicle-treated groups (testing for genotype difference among vehicle-treated groups). *n*=7-8/time point/group for males; and *n*=7-13/time point/group for females.

Figure 5: (**A**) Photomicrographs of whole-bone (left side of panel) and close-up views from a portion of the whole bone images (right side of panel) of representative midshaft femur sections from male Cre-negative and ^{10kb}Dmp1-Cre positive Lrp5$^{f/f}$;Lrp6$^{f/f}$ compound mice at 14.5 wks of age, treated with (mAb) or without (veh) sclerostin antibody for 10 wks prior to sacrifice. The fluorochrome labels calcein (green), oxytetracycline (yellow), alizarin complexone (red), and demeclocycline (orange) were sequentially injected throughout the experimental period to mark the position of the forming bone surface at various points for later quantification of bone formation parameters. Quantitation of (**B**) periosteal mineralizing surface (Ps.MS/BS), (**C**) periosteal mineral apposition rate (Ps.MAR), and (**D**) periosteal bone formation rate per unit bone surface (PS.BFR/BS). Panels **E**-**F** quantitate the same measurements for the endocortical surface. Data were tested for significance using two-way ANOVA, with Cre status and injection type as main effects. P-values for individual main effects and for the interaction term are presented in each panel. Tukey's HSD post hoc tests were used to compare among groups. *p<0.05 for comparison to respective vehicle-treated group (within Cre genotype). †p<0.05 for comparison between vehicle-treated groups (testing for genotype difference among vehicle-treated groups). *n*=5-7/group.

Figure 6: ELISA-based quantification the bone resorption marker carboxy-terminal collagen crosslinks (CTX) from Cre-negative and ^{10kb}Dmp1-Cre positive Lrp5$^{f/f}$;Lrp6$^{f/f}$ compound mice at 4 wks (black bars) and 6.5 wks (grey bars) of age, treated with (mAb) or without (veh) sclerostin antibody beginning at 4.5 wks of age. (**A**) males; (**B**) females. Data were tested for significance using two-way ANOVA, with Cre status and injection type as main effects. P-values for individual main effects and for the interaction term are presented in each panel. Post-hoc tests were not performed due to failure of omnibus ANOVA to detect any significant differences for any individual or combined effects. *n*=6-7/time point/group for males; and *n*=3/time point/group for females.

Supplemental Figure Captions

Figure S1: Genomic DNA was isolated from liver (left panels) and cleaned cortical bone (right panels) from Cre-negative and ^{10kb}Dmp1-Cre positive Lrp5$^{f/f}$;Lrp6$^{f/f}$ compound mice used in the antibody experiment. PCR was performed on genomic DNA for Lrp6 (upper panels) and Lrp5 (lower panels) amplification, using primer sets that distinguish the wild-

type, intact floxed, and recombined floxed alleles. Recombination of the floxed Lrp5/Lrp6 alleles was not detected in the liver, regardless of Cre status. Cortical bone samples from Cre-positive but not Cre-negative mice yielded a recombined band for both Lrp5 and Lrp6. A band for the unrecombined Lrp5 allele was also evident in Cre+ bone samples despite being homozygous for the floxed Lrp5 allele, which likely reflects failure to exclude cell types other than Dmp1-expressing cells during tissue harvest, preparation, and cleaning. It is likely that a similar signal for the unrecombined Lrp6 band exists in the Cre+ bone reactions, but the large disparity in band size between the recombined (372 bp) and unrecombined (1155 bp) alleles would favor absence of the large band simply because the smaller bands are so much more efficient for amplification during PCR. The unrecombined and recombined Lrp5 bands are very similar in size and thus the unrecombined is more detectable than in the case of Lrp6. The control lane ("ctrl") contains amplified DNA from an $Lrp6^{+/-}$ mouse (upper panels) or an $Lrp5^{+/f}$ mouse (without Cre; lower panels).

Figure S2: Serial body weight measurements for Cre-negative (triangles) and ^{10kb}Dmp1-Cre positive (circles) $Lrp5^{f/f}$;$Lrp6^{f/f}$ compound mice. Weight was collected every 2.5-3 wks. Left panel displays data from male mice; right panel displays data from female mice. Antibody (dashed lines) and vehicle (solid lines) treatment began at 4.5 wks of age and lasted the duration of the experiment (to 14 wks of age). The longitudinal data were tested for significance within sex, between Cre status, using two-way rmANOVA. P-values for individual main effects and for the interaction term are presented in each panel. Tukey's HSD post hoc tests were used to compare among groups, but none of the individual group pairwise comparisons reached statistical significance. *n*=7-9/time point/group for males; and *n*=8-13/time point/group for females.

Figure S3: µCT-derived measurement of the distal femur metaphyseal cancellous bone and mid-femur cortical bone from female Cre-negative and ^{10kb}Dmp1-Cre positive $Lrp5^{f/f}$;$Lrp6^{f/f}$ compound mice at 14.5 wks of age, treated with (mAb) or without (veh) sclerostin antibody for 10 wks prior to sacrifice. Quantitative differences in distal femur (**A**) trabecular bone volume fraction (BV/TV); (**B**), trabecular thickness (Tb.Th), and (**C**) trabecular number (Tb.N). Quantitative differences in midshaft femur cortical bone (**D**) total area (Tt.Ar), (**E**) bone area (B.Ar), and (**F**) cortical thickness. (**G**) Representative 3D reconstructions of (top row) the midshaft femur, (middle row) the distal metaphysis (proximal view), and (bottom row) the caudal half of the distal femur (the ventral half was digitally removed). Male data and reconstructions are presented in Fig. 2. Data were tested for significance using two-way ANOVA, with Cre status and injection type as main effects. P-values for individual main effects and for the interaction term are presented in each panel. Tukey's HSD post hoc tests were used to compare among groups. *$p<0.05$ for comparison to respective vehicle-treated group (within Cre genotype). †$p<0.05$ for comparison between vehicle-treated groups (testing for genotype difference among vehicle-treated groups). *n*=8-13/group.

Figure S4: µCT-derived measurement of the 5th lumbar (L5) vertebral body cancellous bone from female Cre-negative and ^{10kb}Dmp1-Cre positive $Lrp5^{f/f}$;$Lrp6^{f/f}$ compound mice at 14.5 wks of age, treated with (mAb) or without (veh) sclerostin antibody for 10 wks prior to sacrifice. (**A**) Quantitative differences in 5th lumbar trabecular bone volume fraction (BV/TV). Too little trabecular bone was present to take meaningful trabecular thickness and number

measurements via μCT. (**D**) Representative 3D cutaway reconstructions of the 5th lumbar vertebra in rostro-caudal view (top row) and dorsoventral view (bottom row). Male data and reconstructions are presented in Fig. 3. Data were tested for significance using two-way ANOVA, with Cre status and injection type as main effects. P-values for individual main effects and for the interaction term are presented in each panel. Tukey's HSD post hoc tests were used to compare among groups. *p<0.05 for comparison to respective vehicle-treated group (within Cre genotype). †p<0.05 for comparison between vehicle-treated groups (testing for genotype difference among vehicle-treated groups). *n*=8-13/group.

Figure S5: Decalcified thin sections through the distal femur of 14.5-wk-old male mice, reacted for Trap activity (red staining) and counterstained with methyl green. Osteoclasts are visible in all groups, but the lack of spongiosa in the Cre+ mice precluded quantification of osteoclast parameters.

Figure S6: ELISA-based quantification the bone formation inhibitor sclerostin from female Cre-negative and ^{10kb}Dmp1-Cre positive Lrp5$^{f/f}$;Lrp6$^{f/f}$ compound mice at 4 wks (black bars) and 6.5 wks (grey bars) of age, treated with (mAb) or without (veh) sclerostin antibody beginning at 4.5 wks of age. Data were tested for significance using two-way ANOVA, with Cre status and injection type as main effects. P-values for individual main effects and for the interaction term are presented in each panel. Tukey's HSD post hoc tests were used to compare among groups. It should be noted that the highest concentration of sclerostin standard that is supplied with the R&D Systems kit is 1000 ng/mL. The antibody-treated groups exhibited >2x that amount, so those values are log-linear extrapolations lying outside the range of the standard curve. *p<0.05 for comparison to respective vehicle-treated group (within Cre genotype and time point). †p<0.05 for comparison between vehicle-treated groups (testing for genotype difference among vehicle-treated groups). *n*=5/group.

References Cited

1. Aspray TJ & Hill TR (2019) Osteoporosis and the Ageing Skeleton. *Subcell Biochem* 91:453-476
2. Foundation NO (2020) Osteoporosis Fast Facts. *NOF* https://cdn.nof.org/wp-content/uploads/2015/12/Osteoporosis-Fast-Facts.pdf
3. Miller PD, Hattersley G, Riis BJ, Williams GC, Lau E, Russo LA, . . . Investigators AS (2016) Effect of Abaloparatide vs Placebo on New Vertebral Fractures in Postmenopausal Women With Osteoporosis: A Randomized Clinical Trial. *JAMA* 316(7):722-733
4. Saag KG, Petersen J, Brandi ML, Karaplis AC, Lorentzon M, Thomas T, . . . Grauer A (2017) Romosozumab or Alendronate for Fracture Prevention in Women with Osteoporosis. *N Engl J Med* 377(15):1417-1427
5. Brunkow ME, Gardner JC, Van Ness J, Paeper BW, Kovacevich BR, Proll S, . . . Mulligan J (2001) Bone dysplasia sclerosteosis results from loss of the SOST gene product, a novel cystine knot-containing protein. *Am J Hum Genet* 68(3):577-589. PMC1274471.
6. Balemans W, Ebeling M, Patel N, Van Hul E, Olson P, Dioszegi M, . . . Van Hul W (2001) Increased bone density in sclerosteosis is due to the deficiency of a novel secreted protein (SOST). *Hum Mol Genet* 10(5):537-543
7. Boyden LM, Mao J, Belsky J, Mitzner L, Farhi A, Mitnick MA, . . . Lifton RP (2002) High bone density due to a mutation in LDL-receptor-related protein 5. *N Engl J Med* 346(20):1513-1521
8. Little RD, Carulli JP, Del Mastro RG, Dupuis J, Osborne M, Folz C, . . . Johnson ML (2002) A mutation in the LDL receptor-related protein 5 gene results in the autosomal dominant high-bone-mass trait. *Am J Hum Genet* 70(1):11-19. PMC419982.
9. Semenov MV & He X (2006) LRP5 mutations linked to high bone mass diseases cause reduced LRP5 binding and inhibition by SOST. *J Biol Chem* 281(50):38276-38284
10. Semenov M, Tamai K & He X (2005) SOST is a ligand for LRP5/LRP6 and a Wnt signaling inhibitor. *J Biol Chem* 280(29):26770-26775
11. Cui Y, Niziolek PJ, MacDonald BT, Zylstra CR, Alenina N, Robinson DR, . . . Robling AG (2011) Lrp5 functions in bone to regulate bone mass. *Nat Med* 17(6):684-691. PMC3113461.
12. Li X, Ominsky MS, Niu QT, Sun N, Daugherty B, D'Agostin D, . . . Paszty C (2008) Targeted deletion of the sclerostin gene in mice results in increased bone formation and bone strength. *J Bone Miner Res* 23(6):860-869
13. Niziolek PJ, Farmer TL, Cui Y, Turner CH, Warman ML & Robling AG (2011) High-bone-mass-producing mutations in the Wnt signaling pathway result in distinct skeletal phenotypes. *Bone* 49(5):1010-1019. PMC3412139.
14. Frost M, Andersen T, Gossiel F, Hansen S, Bollerslev J, van Hul W, . . . Brixen K (2011) Levels of serotonin, sclerostin, bone turnover markers as well as bone density and microarchitecture in patients with high-bone-mass phenotype due to a mutation in Lrp5. *J Bone Miner Res* 26(8):1721-1728
15. Holmen SL, Giambernardi TA, Zylstra CR, Buckner-Berghuis BD, Resau JH, Hess JF, . . . Williams BO (2004) Decreased BMD and limb deformities in mice carrying mutations in both Lrp5 and Lrp6. *J Bone Miner Res* 19(12):2033-2040
16. Kubota T, Michigami T, Sakaguchi N, Kokubu C, Suzuki A, Namba N, . . . Ozono K (2008) Lrp6 hypomorphic mutation affects bone mass through bone resorption in mice and impairs interaction with Mesd. *J Bone Miner Res* 23(10):1661-1671
17. Kedlaya R, Veera S, Horan DJ, Moss RE, Ayturk UM, Jacobsen CM, . . . Robling AG (2013) Sclerostin inhibition reverses skeletal fragility in an Lrp5-deficient mouse model of OPPG syndrome. *Sci Transl Med* 5(211):211ra158. PMC3964772.
18. MacDonald BT, Semenov MV, Huang H & He X (2011) Dissecting molecular differences between Wnt coreceptors LRP5 and LRP6. *PLoS One* 6(8):e23537. PMC3160902.
19. Li X, Zhang Y, Kang H, Liu W, Liu P, Zhang J, . . . Wu D (2005) Sclerostin binds to LRP5/6 and antagonizes canonical Wnt signaling. *J Biol Chem* 280(20):19883-19887
20. Holdsworth G, Slocombe P, Doyle C, Sweeney B, Veverka V, Le Riche K, . . . Robinson MK (2012) Characterization of the interaction of sclerostin with the low density lipoprotein receptor-related protein (LRP) family of Wnt co-receptors. *J Biol Chem* 287(32):26464-26477. PMC3410989.
21. Winkler DG, Sutherland MK, Geoghegan JC, Yu C, Hayes T, Skonier JE, . . . Latham JA (2003) Osteocyte control of bone formation via sclerostin, a novel BMP antagonist. *EMBO J* 22(23):6267-6276. PMC291840.
22. Craig TA, Bhattacharya R, Mukhopadhyay D & Kumar R (2010) Sclerostin binds and regulates the activity of cysteine-rich protein 61. *Biochem Biophys Res Commun* 392(1):36-40. PMC2821021.

23. Devarajan-Ketha H, Craig TA, Madden BJ, Robert Bergen H, 3rd & Kumar R (2012) The sclerostin-bone protein interactome. *Biochem Biophys Res Commun* 417(2):830-835. PMC3259242.
24. Craig TA & Kumar R (2010) Sclerostin-erbB-3 interactions: modulation of erbB-3 activity by sclerostin. *Biochem Biophys Res Commun* 402(2):421-424. PMC2992958.
25. Joeng KS, Schumacher CA, Zylstra-Diegel CR, Long F & Williams BO (2011) Lrp5 and Lrp6 redundantly control skeletal development in the mouse embryo. *Dev Biol* 359(2):222-229. PMC3220949.
26. Lu Y, Xie Y, Zhang S, Dusevich V, Bonewald LF & Feng JQ (2007) DMP1-targeted Cre expression in odontoblasts and osteocytes. *J Dent Res* 86(4):320-325
27. Li X, Ominsky MS, Warmington KS, Morony S, Gong J, Cao J, . . . Paszty C (2009) Sclerostin antibody treatment increases bone formation, bone mass, and bone strength in a rat model of postmenopausal osteoporosis. *J Bone Miner Res* 24(4):578-588
28. Bouxsein ML, Boyd SK, Christiansen BA, Guldberg RE, Jepsen KJ & Muller R (2010) Guidelines for assessment of bone microstructure in rodents using micro-computed tomography. *J Bone Miner Res* 25(7):1468-1486
29. Robling AG, Kang KS, Bullock WA, Foster WH, Murugesh D, Loots GG & Genetos DC (2016) Sost, independent of the non-coding enhancer ECR5, is required for bone mechanoadaptation. *Bone* 92:180-188. PMC6673653.
30. Robling AG, Kedlaya R, Ellis SN, Childress PJ, Bidwell JP, Bellido T & Turner CH (2011) Anabolic and catabolic regimens of human parathyroid hormone 1-34 elicit bone- and envelope-specific attenuation of skeletal effects in Sost-deficient mice. *Endocrinology* 152(8):2963-2975. PMC3138236.
31. Dempster DW, Compston JE, Drezner MK, Glorieux FH, Kanis JA, Malluche H, . . . Parfitt AM (2013) Standardized nomenclature, symbols, and units for bone histomorphometry: a 2012 update of the report of the ASBMR Histomorphometry Nomenclature Committee. *J Bone Miner Res* 28(1):2-17. PMC3672237.
32. Kedlaya R, Kang KS, Hong JM, Bettagere V, Lim KE, Horan D, . . . Robling AG (2016) Adult-Onset Deletion of beta-Catenin in (10kb)Dmp1-Expressing Cells Prevents Intermittent PTH-Induced Bone Gain. *Endocrinology* 157(8):3047-3057. PMC4967118.
33. Bullock WA, Hoggatt AM, Horan DJ, Elmendorf AJ, Sato AY, Bellido T, . . . Robling AG (2019) Lrp4 Mediates Bone Homeostasis and Mechanotransduction through Interaction with Sclerostin In Vivo. *iScience* 20:205-215. PMC6817631.
34. Riddle RC, Diegel CR, Leslie JM, Van Koevering KK, Faugere MC, Clemens TL & Williams BO (2013) Lrp5 and Lrp6 exert overlapping functions in osteoblasts during postnatal bone acquisition. *PLoS One* 8(5):e63323. PMC3651091.
35. Chang MK, Kramer I, Keller H, Gooi JH, Collett C, Jenkins D, . . . Kneissel M (2014) Reversing LRP5-dependent osteoporosis and SOST deficiency-induced sclerosing bone disorders by altering WNT signaling activity. *J Bone Miner Res* 29(1):29-42
36. Kim SW, Lu Y, Williams EA, Lai F, Lee JY, Enishi T, . . . Wein MN (2017) Sclerostin Antibody Administration Converts Bone Lining Cells Into Active Osteoblasts. *J Bone Miner Res* 32(5):892-901. PMC5413385.

CRediT author statement

Conceptualization: Robling, Williams, Warman. Data collection: Lim, Bullock, Horan. Writing: Lim, Robling. Review and Editing: Robling, Lim, Warman, Williams.

HIGHLIGHTS

-I understand that the Highlights section is optional and we have chosen not to submit this page.

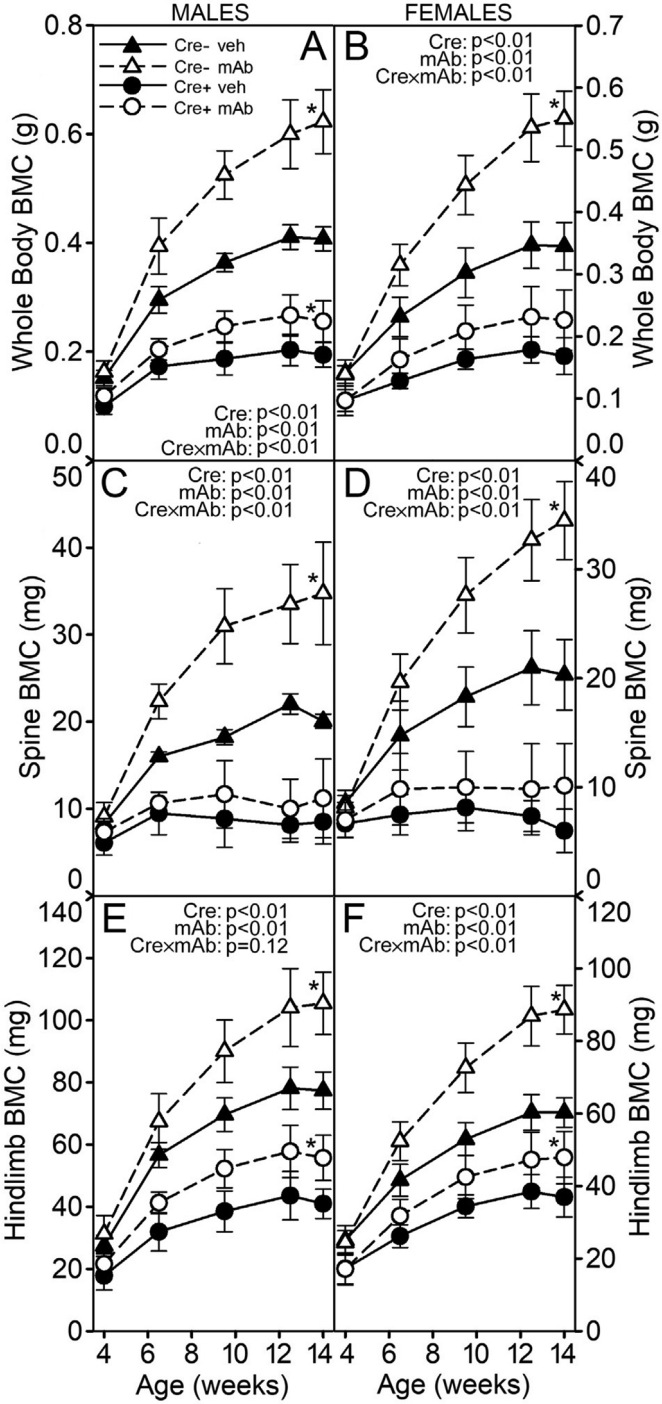
MALES
FEMALES
Cre- veh
Cre- mAb
Cre+ veh
Cre+ mAb
A
B
C
D
E
F
Cre: p<0.01
mAb: p<0.01
Cre×mAb: p<0.01
Cre: p<0.01
mAb: p<0.01
Cre×mAb: p=0.12
Whole Body BMC (g)
Spine BMC (mg)
Hindlimb BMC (mg)
Age (weeks)
Age (weeks)

Figure 1

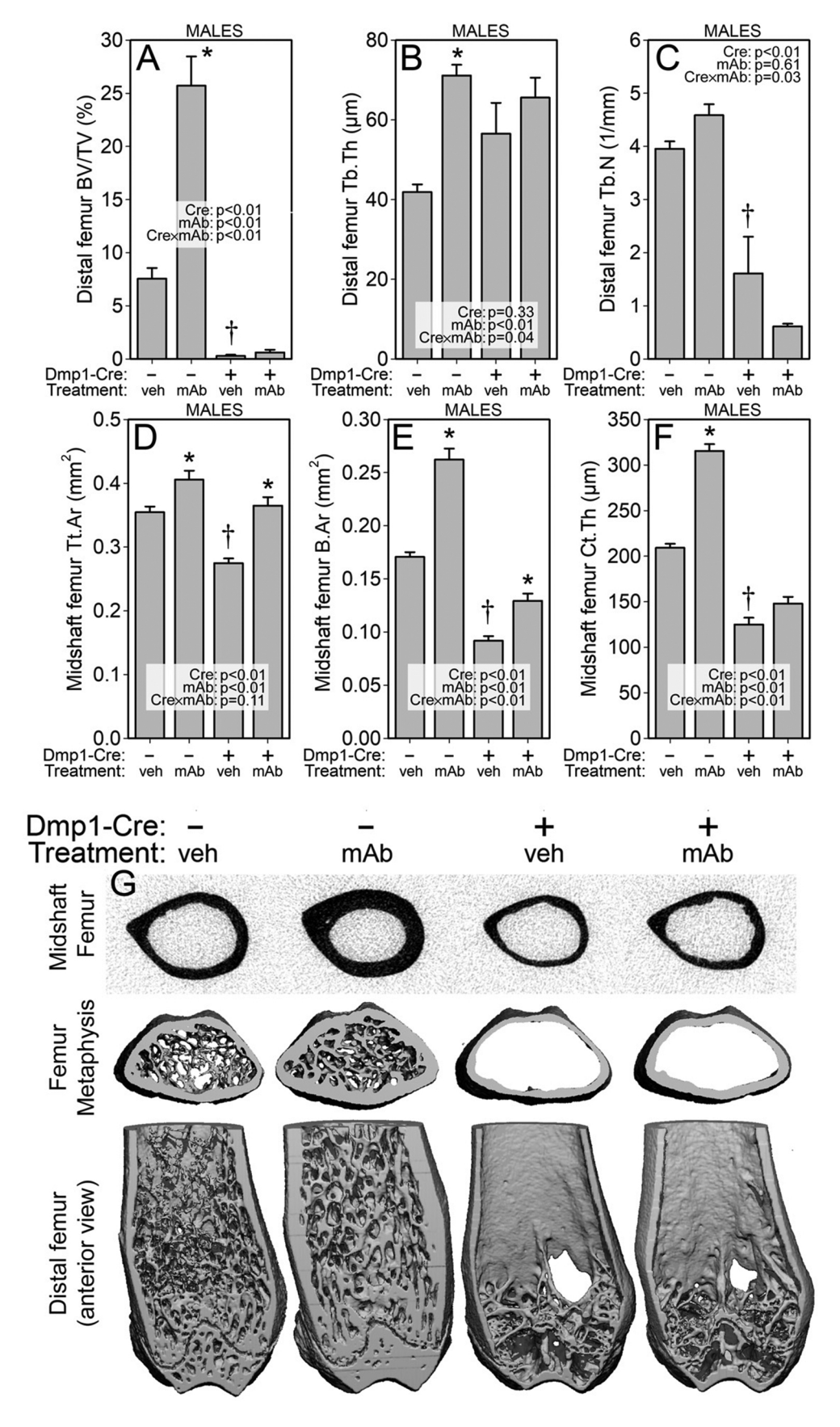
MALES
A
Distal femur BV/TV (%)
Cre: p<0.01
mAb: p<0.01
Cre×mAb: p<0.01
B
Distal femur Tb.Th (μm)
Cre: p=0.33
mAb: p<0.01
Cre×mAb: p=0.04
C
Distal femur Tb.N (1/mm)
Cre: p<0.01
mAb: p=0.61
Cre×mAb: p=0.03
D
Midshaft femur Tt.Ar (mm²)
Cre: p<0.01
mAb: p<0.01
Cre×mAb: p=0.11
E
Midshaft femur B.Ar (mm²)
Cre: p<0.01
mAb: p<0.01
Cre×mAb: p<0.01
F
Midshaft femur Ct.Th (μm)
Cre: p<0.01
mAb: p<0.01
Cre×mAb: p<0.01
Dmp1-Cre: – – + +
Treatment: veh mAb veh mAb
G
Midshaft Femur
Femur Metaphysis
Distal femur (anterior view)

Figure 2

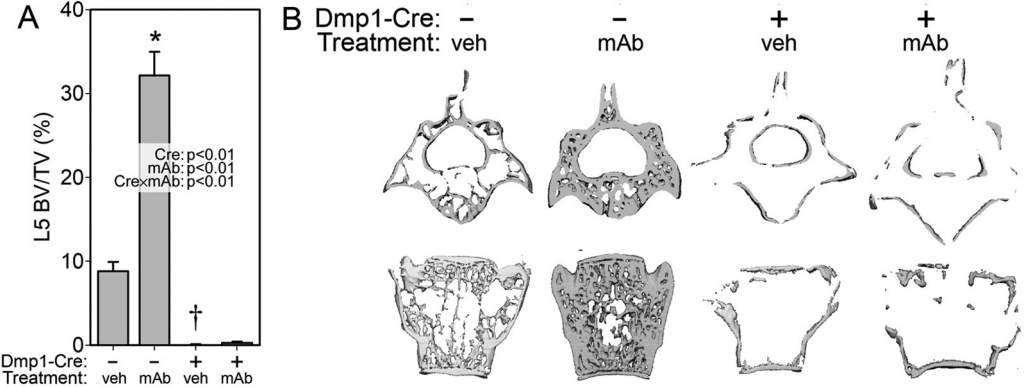
A
40
30
20
10
0
L5 BV/TV (%)
*
†
Cre: p<0.01
mAb: p<0.01
Cre×mAb: p<0.01
Dmp1-Cre: – – + +
Treatment: veh mAb veh mAb
B
Dmp1-Cre: – – + +
Treatment: veh mAb veh mAb

Figure 3

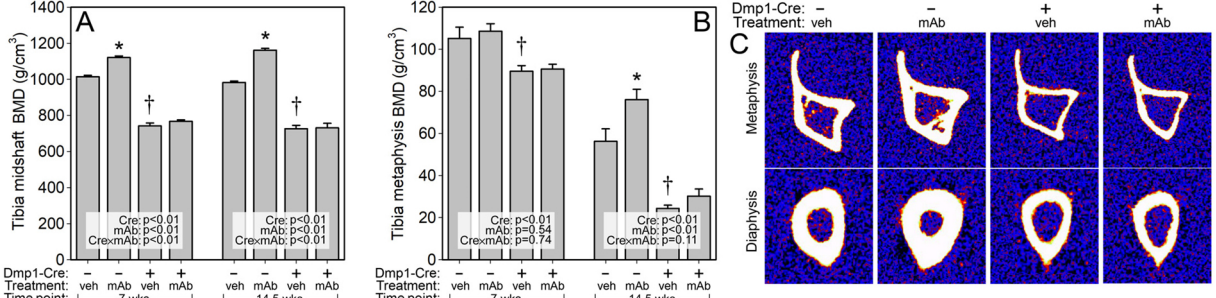
A
Tibia midshaft BMD (g/cm3)
1400
1200
1000
800
600
400
200
0
Cre: p<0.01
mAb: p<0.01
Cre×mAb: p<0.01
Cre: p<0.01
mAb: p<0.01
Cre×mAb: p<0.01
Dmp1-Cre: – – + + – – + +
Treatment: veh mAb veh mAb veh mAb veh mAb
Time point: 7 wks 14.5 wks
B
Tibia metaphysis BMD (g/cm3)
120
100
80
60
40
20
0
Cre: p<0.01
mAb: p=0.54
Cre×mAb: p=0.74
Cre: p<0.01
mAb: p<0.01
Cre×mAb: p=0.11
Dmp1-Cre: – – + + – – + +
Treatment: veh mAb veh mAb veh mAb veh mAb
Time point: 7 wks 14.5 wks
C
Dmp1-Cre: – – + +
Treatment: veh mAb veh mAb
Metaphysis
Diaphysis

Figure 4

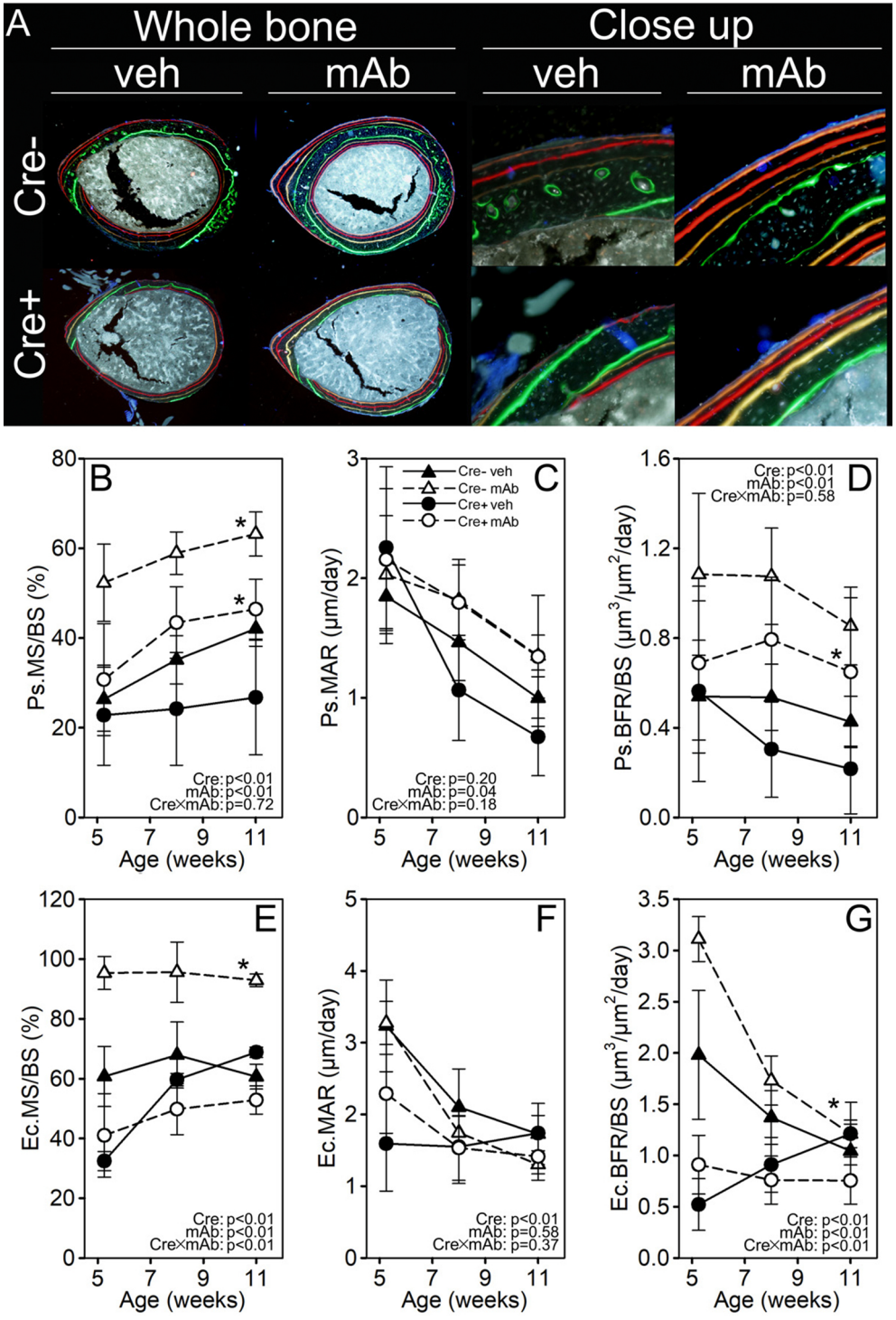
A
Whole bone
Close up
veh
mAb
veh
mAb
Cre-
Cre+
B
Ps.MS/BS (%)
Cre: p<0.01
mAb: p<0.01
Cre×mAb: p=0.72
Age (weeks)
C
Cre- veh
Cre- mAb
Cre+ veh
Cre+ mAb
Ps.MAR (µm/day)
Cre: p=0.20
mAb: p=0.04
Cre×mAb: p=0.18
Age (weeks)
D
Cre: p<0.01
mAb: p<0.01
Cre×mAb: p=0.58
Ps.BFR/BS (µm³/µm²/day)
Age (weeks)
E
Ec.MS/BS (%)
Cre: p<0.01
mAb: p<0.01
Cre×mAb: p<0.01
Age (weeks)
F
Ec.MAR (µm/day)
Cre: p<0.01
mAb: p=0.58
Cre×mAb: p=0.37
Age (weeks)
G
Ec.BFR/BS (µm³/µm²/day)
Cre: p<0.01
mAb: p<0.01
Cre×mAb: p<0.01
Age (weeks)

Figure 5

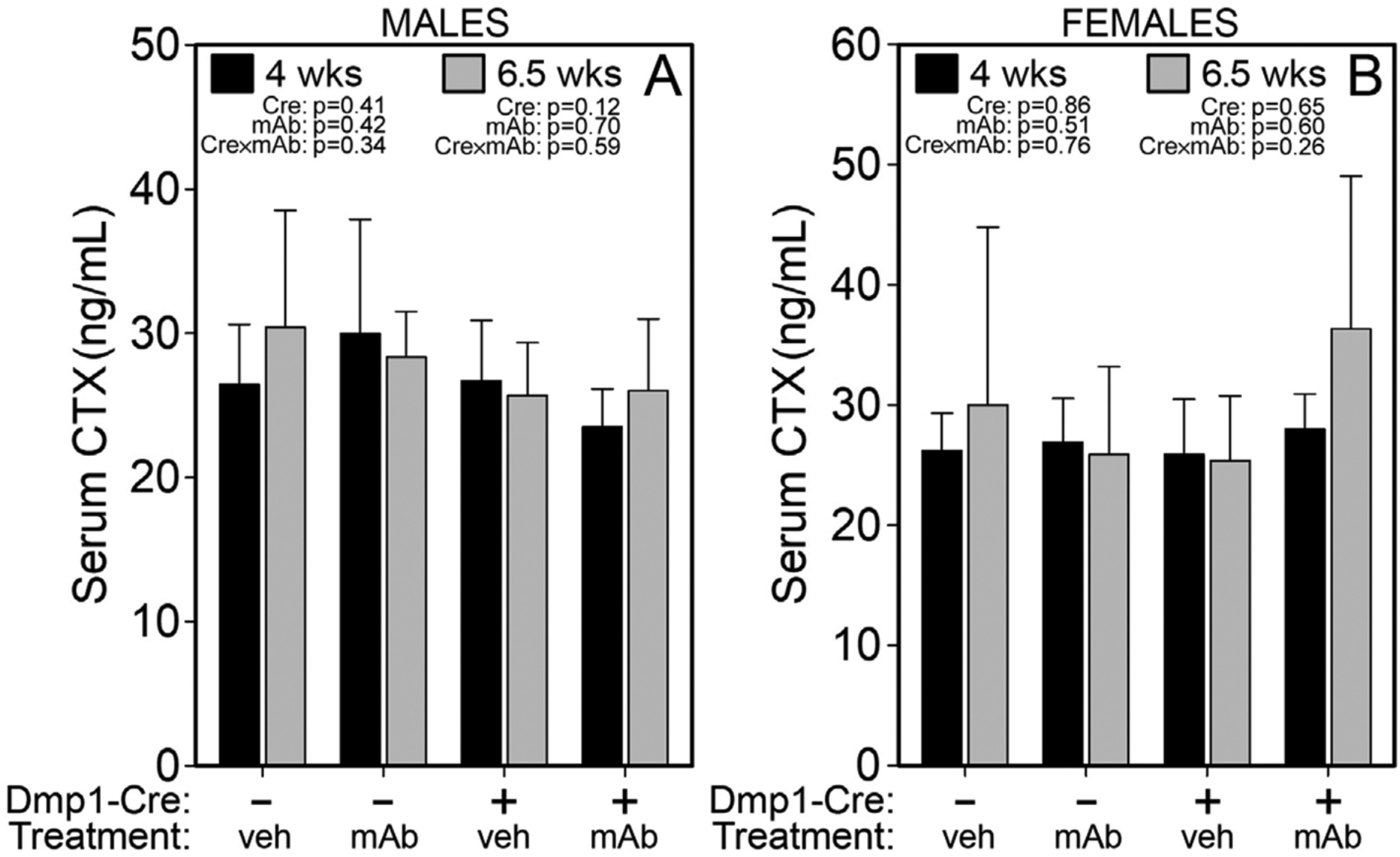
MALES
4 wks
6.5 wks
A
Cre: p=0.41
mAb: p=0.42
CrexmAb: p=0.34
Cre: p=0.12
mAb: p=0.70
CrexmAb: p=0.59
Serum CTX (ng/mL)
0
10
20
30
40
50
Dmp1-Cre: − − + +
Treatment: veh mAb veh mAb
FEMALES
4 wks
6.5 wks
B
Cre: p=0.86
mAb: p=0.51
CrexmAb: p=0.76
Cre: p=0.65
mAb: p=0.60
CrexmAb: p=0.26
Serum CTX (ng/mL)
0
10
20
30
40
50
60
Dmp1-Cre: − − + +
Treatment: veh mAb veh mAb

Figure 6